A Density Functional Theory Study on the Water Aggregation Behaviour of Fatty-Acid Based Anionic Surface Active Ionic Liquids

Suresh Sampathkumar
Bharathiar University
Subramaniam Vijayakumar (svijayakumar@buc.edu.in)
Bharathiar University https://orcid.org/0000-0002-7287-1177

Research Article

Keywords: Ionic Liquids, Methyl-Imidazolium Cation, Fatty-Acid Anion, Density Functional Theory, Water Cluster

Posted Date: December 6th, 2021

DOI: https://doi.org/10.21203/rs.3.rs-1114721/v1

Version of Record: A version of this preprint was published at Structural Chemistry on March 15th, 2022.
See the published version at https://doi.org/10.1007/s11224-022-01910-6.

Abstract

The hydrogen bond interactions between methyl-imidazolium cation (MIM^+) and fatty-acid anions ($C_mH_nCOO^-$, where m=1–6; n-3–13) of ionic liquids are studied in both gas phase and water phase using density functional theory. The structural properties show that the presence of N–H···O and C–H···O hydrogen bonds between $[MIM]^+$ and $[C_mH_nCOO]^-$ (m=1–6;n-3–13) ionic liquids. From the vibrational frequency analysis it was found that the hydrogen bond interaction between $[MIM]^+$ and $[C_mH_nCOO]^-$ (m=1–6;n-3–13) ionic liquids are red-shifted in frequency. The natural bond orbital analysis show that the N–H···O hydrogen bond associated with the large charge transfer which has the higher stabilization energy (*i.e.* $E^{(2)} \sim 38$ kcal/mol). Further, the cation/anion–water cluster $(H_2O)_{1\text{-}3}$ interactions show that the water molecules are preferred to interact with anions. In the case of ionic liquids–water cluster interaction, the water molecules occupies the interstitial space between cation and anion of ionic liquids which results in weakening the cation-anion interaction.

1. Introduction

Ionic liquids (ILs) are a class of organic salts composed of ions that are exist in the liquid state at low temperatures (below 100 °c) [1–8]. Generally, ILs consists of organic cation (for example, imidazolium, pyridinium, phosphonium and etc.,) and organic/inorganic anion (for example, acetate, nitrate, tetrafuoroborate, alkyl-sulfate and etc.,) [9–19]. Because of their unique properties, they have attracted research interests in both academia and industries as they applied in organic/inorganic synthesis, catalysis, electrochemical devices and so on [20–26]. Different kinds of ILs are developed and studied for various applications such as room-temperature ionic liquids (RTILs) [2, 16, 27], poly-ionic liquids (PILs) [28, 29], amino-acid ionic iquids (AAILs) [30–32] and task-specific ionic liquids (TSILs) [33, 34]. Similarly, new class of ionic liquid called surface active ionic liquid (SAILs) have possess diverse applications in organic synthesis, biotechnology, nanotechnology, surfactant flooding and so on [35–39]. It is considered that the SAILs have both the properties of ILs and surfactant. Based on the structural property, SAILs can be divided into three category, (i) cationic SAILs (like imidazolium, pyridinium with long alkyl chain), (ii) anion SAILs (like carboxylate anion, sulphate anion and sulfonate anion) and (iii) catanionic SAILs (cations and anions showing surface active properties) [38, 39]. The nature of SAILs can be tuned by the choice of cation and anion, and the properties of SAILs are studied extensively in colloidal chemistry, supramolecular chemistry, eletrochemisty, pharmaceutical industry and etc., [40–43]

The presence of hydrogen bond (H-bond) between cation and anion of ILs plays a vital role in the behaviour of ILs [44–48]. In general, the H-bond is denoted as X–H···Y interaction in which X (usually, C, N and O) and Y (usually, N and O) are strong electronegative atoms. It was found that the cations are the active H-bond donors and anions are the active H-bond acceptors. Based on the strength of the H-bond, the ILs are divided into two types, (i) protic ILs and (ii) aprotic ILs. In protic ILs, H-bond is formed by proton transfer from a Brønsted acid to a Brønsted base whereas in aprotic ILs, the cationic C–H unit be the major H-bond donor unit [48]. Since, ILs have large numbers of cations and anions, the H-bonding in

ILs are highly system dependent. Unlike, the H-bonding in traditional neutral system, the H-bonding present in the ILs have different interesting behaviours.

Nowadays, the water aggregation or micellization properties of SAILs are actively studied by both experimental and theoretical studies [38, 49, 50]. Experimentally, surface tension, conductivity, steady state fluorescence spectra, viscosity, and dynamic light scattering measurements are used to determine the water aggregation properties of SAILs. Theoretically, density functional theory (DFT) is used to study the water aggregation properties of SAILs. Mostly, the studies are performed on water aggregation properties of imidazolium cations with sulfonate anions of SAILs [39, 51]. It promoted us to study the water aggregation properties of SAILS. Here, we have studied the water aggregation properties of the methyl-imidazolium cation with six fatty-acid anion of SAILs with different water molecules (1–3) using DFT. This study will be useful to understand the interactions of cation-water, anion-water, cation-anion and ionic liquid-water towards the water aggregation properties of SAILs.

2. Computational Details

The hybrid M06-2X density functional [52] along with 6-311++G (d,p) basis set [53] is used to optimize the structures of methyl-imidazolium cation $[MIM]^+$, fatty-acid based anions $[C_mH_nCOO]^-$ (where, m=1–6; n=3–13) and ILs $[MIM^+–C_mH_nCOO^-]$ (m=1–6; n=3–13) and ILs with water molecules $(H_2O)_x$ (where, x=1–3) respectively. The solvent effects on the stability of ILs are examined through self-consistent reaction field (SCRF) using polarizable continuum model (PCM) in water [54, 55]. Vibrational frequency analysis used to found the global minimum structures with no imaginary frequency values. The strength of H-bond between cation and anion of ILs are studied by atoms in molecule (AIM) analysis using the MORPHY98 program package [56, 57]. Further, the natural bond orbital (NBO) analysis is used to understand the charge transfer between ILs [58]. All, the above calculations are performed with Gaussian09 Rev. A.02 package [59].

3. Results And Discussion

3.1 Structures of $[MIM]^+$ Cation and $[C_mH_nCOO]^-$ Anions

The optimized structures of methyl-imidazolium cation $[MIM]^+$ and fatty-acid anions $[C_mH_nCOO]^-$ (where, m=1–6; n=3–13) are shown in Figure 1. In the case of $[MIM]^+$ cation, a three-center (N1-C2-N3) four-electron $\prod$ system is observed [60]. The bond length of N1=C2 and C2=N3 are predicted to be 1.327 Å and 1.333 Å and the bond length of N3-C4 and C5-N is to be 1.376 Å and 1.381 Å respectively, while for C4=C5 it is of 1.357 Å. From the NBO charge analysis, it is found that the negative charge is located on the two N atoms (N1=-0.35 e and N3=-0.50 e) and positive charge is located on the C2 atom while C4 and C5 atoms have nearly neutral charge. In the case of fatty-acid anions (*i.e.* $[C_mH_nCOO]^-$, where m=1–6; n=3–13)), as the chain length increases (*i.e.* C_1 to C_6) the anions prefers to form bent structure. The natural charge value of −0.81 e is found on the two O atoms (COO^-) in the fatty-acid anions. The length

of the hydrophobic chain in fatty-acid anion is in the range of 2.66–9.65 Å which is in agreement with the theoretically calculated value (2.76–9.09 Å) by Tanford equation, L = 1.5 + 1.265n (where, n is the number of carbon atom) [61].

3.2 Structures of Cation–Water and Anion–Water interactions

The optimized structures of water clusters $(H_2O)_x$ (x=1–3), $[MIM]^+$ cation and $[C_mH_nCOO]^-$ anions (m=1–6; n=3–13) with different water molecules $(H_2O)_x$ (x=1–3) are shown in Figures 2–4 respectively. The purpose of this study is to analyse the changes in the natural charge values of cation and anions of ILs during the interactions with water molecule and also to find the water aggregation property of cation and anions of ILs with water molecule. Previously, Roohi et al. studied the water aggregation property of $[MIM]^+$ cation [62]. The O atom in H_2O molecule forms H-bond with $[MIM]^+$ cation in three ways 1:1, 2:1 and 3:1 ratio. That is, the number of H-bonds between $[MIM]^+$ cation and water molecule is increased with increase of number of water molecules from 1 to 3. The bond length of N3–H13 is elongated from 1.012 Å (cation) to 1.030 Å (cation-water) because of the electron absorption effect of H_2O. The negative charge of N3 atom in $[MIM]^+$ cation is increased from −0.498 e to −0.513 e during the interactions with water molecules $(H_2O)_{1-3}$. Figure 4 shows the optimized structures of interactions between fatty-acid anion with different water molecules $(H_2O)_{1-3}$. Recently, Ali et al. have studied the aggregation behaviour of choline-fatty-acid based ILs by experimentally [63]. Here, the H atom in H_2O molecule forms H-bond with O atom of $[C_mH_nCOO]^-$ (m=1–6; n=3–13) anions in three ways 2:1, 3:1 and 4:1 ratio. The O–C bond of $[C_mH_nCOO]^-$ (m=1–6; n=3–13) anions is increased from 1.249 Å to 1.257 Å during the interactions with water molecule $(H_2O)_{1-3}$. This means that the hydrate formation weakens the O–C bond in the fatty-acid anions. Also, the negative charge of O atom in $[C_mH_nCOO]^-$ (m=1–6; n=3–13) anions are increased from −0.81 e to −0.84 e on interactions with H atom of water molecules $(H_2O)_{1-3}$.

3.3 Structures of Cation–Anion interactions

The optimized structures of ILs $[MIM]^+$–$[C_1H_3COO]^-$, $[MIM]^+$–$[C_2H_5COO]^-$, $[MIM]^+$–$[C_3H_7COO]^-$, $[MIM]^+$–$[C_4H_9COO]^-$, $[MIM]^+$–$[C_5H_{11}COO]^-$ and $[MIM]^+$–$[C_6H_{13}COO]^-$ are shown in Figure 5 and Figures S1–S3. The methyl-imidazolium cation $[MIM]^+$ shows different interaction sites for the fatty-acid anions $[C_mH_nCOO]^-$ (m=1–6; n=3–13). In this study, four different interaction sites are considered (site i) C2-N3, (site ii) N3-C4, (site iii) N3 and (site iv) N1-C2 (Figures 5 and S1–S3). Further, the optimized structures of ion-pairs in water phase and ion-pair without proton transfer is shown in Figures S4 and S5. Among that, the C2-N3 site of MIM^+ cation is the preferred site for the interaction of fatty-acid anions (Figure 5). From the NBO natural charge analysis, it is evident that the C2 atom in the C2-N3 site has more positive charge compare to the other possible sites which leads to the much stronger interactions with the anions. As shown in Figure 5, there are two H-bonds are formed (i.e. N–H···O and C–H···O) between $[MIM]^+$ and $[C_mH_nCOO]^-$ (m=1–6;n-3–13). The calculated bond length, bond angle values of H-bond between $[MIM]^+$

and $[C_mH_nCOO]^-$ (m=1–6;n-3–13) are listed in Table 1. The H-bond distance of N–H···O and C–H···O are in the range of 1.692 – 1.704 Å and 2.300 – 2.310 Å respectively. During cation–anion interaction, the N3–H13 and C2–H9 bond in the $[MIM]^+$ cation is elongated by 0.692 Å and 0.020 Å. The obtained result is in agreement with the previous result in which the N–H bond of $[MIM]^+$ cation is elongated by 0.670 Å while interacting with $[C_1H_3COO]^-$ anion [62]. This result shows that the proton transfer takes place from N–H bond of $[MIM]^+$ cation to $[C_mH_nCOO]^-$ anion (m=1–6;n-3–13). The optimized ion-pairs without proton transfer is shown in Figure S5. The calculated relative energy values in Table S1 show that the ion-pairs with proton transfer are much lower in energy compare to the ion-pairs without proton transfer. The bond angle values show that the N–H···O H-bond is almost linear with the bond angle of 175° and the N–H···O H-bond has a bond angle of 122°. The calculated NBO natural charge values shows that, the negative charge in the N3 atom of $[MIM]^+$ cation is increased from –0.50e to –0.58e and the positive charge in the C2 atom of $[MIM]^+$ cation is decreased from +0.30e to +0.24e during the interaction between cation and anion. Correspondingly, the negative charge of both O atoms in the $[C_mH_nCOO]^-$ (m=1–6;n-3–13) anions decreased from –0.81e to –0.70e. This shows that the charge is transferred from the anion unit to cation during the interaction. The optimized structures of ILs ($[MIM]^+$–$[C_mH_nCOO]^-$ (where, m=1–6;n-3–13)) in the water phase is shown in Figure S4. Similar to the gas phase structures, two types of H-bonds found (i.e. N–H···O and C–H···O) between $[MIM]^+$ and $[C_mH_nCOO]^-$ (m=1–6;n-3–13). The H-bond distance of N–H···O and C–H···O are in the range of 1.598 – 1.600 Å and 2.525 – 2.530 Å respectively. During cation–anion interaction, it is noted that the N3–H13 bond in the $[MIM]^+$ cation is elongated by 0.588 Å. The calculated NBO natural charge values shows that, the negative charge in the N3 atom of $[MIM]^+$ cation is increased from –0.50e to –0.57e.

Table 1
The bond length (in Å), bond angle (in °), electron density ρ(r) (in a.u.), Laplacian of electron density $\nabla^2\rho(r)$ (in a.u.) and hessian at bond critical point (H_{BCP}) for the $[MIM]^+$–$[C_mH_nCOO]^-$ (m=1–6; n=3–13) ionic liquids.

ILs	Bond type	Bond length	Bond angle	ρ(r)	$\nabla^2\rho(r)$	H_{BCP}
$[MIM]^+$–$[C_1H_3COO]^-$	N–H···O	1.693	174.83	0.05295	0.10516	−0.01190
	C–H···O	2.310	122.14	0.01347	0.04995	0.00187
$[MIM]^+$–$[C_2H_5COO]^-$	N–H···O	1.692	174.96	0.05301	0.10511	−0.01195
	C–H···O	2.303	122.47	0.01365	0.05065	0.00189
$[MIM]^+$–$[C_3H_7COO]^-$	N–H···O	1.696	174.84	0.05252	0.10516	−0.01164
	C–H···O	2.300	122.59	0.01373	0.05099	0.00191
$[MIM]^+$–$[C_4H_9COO]^-$	N–H···O	1.700	174.67	0.05196	0.10539	−0.01125
	C–H···O	2.300	122.54	0.01369	0.05102	0.00192
$[MIM]^+$–$[C_5H_{11}COO]^-$	N–H···O	1.704	174.63	0.05151	0.10532	−0.01098
	C–H···O	2.293	122.74	0.01388	0.05188	0.00195
$[MIM]^+$–$[C_6H_{13}COO]^-$	N–H···O	1.699	174.92	0.05216	0.10558	−0.01138
	C–H···O	2.310	122.50	0.01344	0.04978	0.00186

3.4 Structures of ILs-Water cluster interactions

The optimized structures of cation–anion of ILs, are further investigated for the water aggregation property with different numbers of water molecules (H_2O_n, n=1–3). The optimized structures of ILs with water molecules are shown in Figure 6–8 respectively. From the Figure 6–8, we found that the water molecules preferentially interact with ILs via C2 site of $[MIM]^+$ cation and COO^- region of fatty-acid anions. The addition of water molecules to the ILs occupies the interstitial part of cation–anion which further weakened the interaction between cation–anion. Previous study also mentioned that the introduction of water molecules reduced the interaction of cation and anion of ILs [48]. Both $[MIM]^+$ cations and $[C_mH_nCOO]^-$ (m=1–6;n-3–13) anions forms multiple H-bonds with water molecules (Figure 6–8). The $[MIM]^+$ cations forms H-bond via C–H···O and the fatty-acid $[C_mH_nCOO]^-$ (m=1–6;n-3–13) anions forms H-bond via O–H···O interactions with the water molecules. It was found that the water molecules prefers to bind with the fatty-acid anions rather than the $[MIM]^+$ cations [32, 64].

3.5 Vibrational Frequency analysis

The strength of interaction between cation and anions in ILs can be identified by Infra-red (IR) spectra analysis. The frequency analysis of X–H···Y H-bond is important to characterize their nature, whether the X–H bonds are proper or improper *i.e.* red shifted or blue shifted. The H-bond formation leads to increase in the X–H bond length because of the proton donor (X), as a result of red-shift is observed in the X–H stretching frequencies. On the other hand, the contraction of X–H bond length will give blue-shift H-bonds. The N–H bond stretching frequency in the isolated $[MIM]^+$ cation is calculated as 3636 cm^{-1} which is in agreement with the experimental value of 3518 cm^{-1} [65]. During the $[MIM]^+$–water interaction, the addition of water molecules $(H_2O)_{1-3}$ leads to red-shift in N–H bond stretching frequencies in the $[MIM]^+$ cation from 393 cm^{-1} to 434 cm^{-1}. This is due to the presence of water molecules produces higher flexibility to the $[MIM]^+$ cation ring [66]. Similarly, the fatty-acid anion–water interactions leads to increase in the bond length of C–O in the $[C_mH_nCOO]^-$ (m=1–6; n=3–13) anions which corresponds to the red-shift H-bonds. In the case of $[MIM]^+$– $[C_mH_nCOO]^-$ interactions, there are two types of H-bonds found (*i.e.* N–H···O and C–H···O). The N–H bond in $[MIM]^+$ cation is red-shifted by 634–659 cm^{-1} during the $[MIM]^+$– $[C_mH_nCOO]^-$ interactions. The C–H bond stretching frequency in the isolated $[MIM]^+$ cation is calculated as 3293 cm^{-1} which is in agreement with the experimental value 3160 cm^{-1} [65]. The C–H bond in $[MIM]^+$ cation is also red-shifted by 13–47 cm^{-1} during the $[MIM]^+$–$[C_mH_nCOO]^-$ interactions. Further, the nature of H-bond is investigated for the interactions of $[MIM]^+$ $[C_mH_nCOO]^-$–Water molecules. The addition of water molecules (*i.e.* $(H_2O)_{1-3}$) causes the N–H bond of $[MIM]^+$ cation to blue-shift by 10–335 cm^{-1}. On the other hand, the red-shift nature of C–H bond in $[MIM]^+$ cation is maintained same during the interactions with water molecule $(H_2O)_{1-3}$. This may be due to that the addition of water molecules (*i.e.* $(H_2O)_{1-3}$) occupies the interstitial space between cation and anion and makes the change in its H-bonding nature which is responsible for the above results.

3.6 Interaction energy

One of the advantage of theoretical methods is that the calculation of interaction energy of ILs which plays a vital role in understanding the structure–energetic properties of ILs. The interaction energy can be calculated as the difference between the energy of a total system E_{AB} (example, Cation–Anion of ILs and ILs–Water) and the energy of isolated systems E_A and E_B (example, Cation, Anion, Water).

$$E_{int} = [E_{AB} - (E_A + nE_B)]$$

In this study, the calculated zero point corrected interaction energy between Cation–Water, Anion–Water, Cation–Anion and ILs–Water are shown in Figure 9–11. The total interaction energy ranges from -15 kcal/mol to -140 kcal/mol for the systems considered in this study. In the case of cation–water and anion–water interactions, the total interaction energy is increased by the addition of 1 to 3 water molecules. Especially, the total interaction energy is large in the anion–water interaction than the cation–water interaction which infers that the water molecules prefer to interact with the anion systems (*i.e.* $[C_mH_nCOO]^-$ (m=1–6; n=3–13)) (Figure 9). In general, the fatty-acid anion with carboxyl functional group

(COO^-) is preferred interaction site for the water molecules. The increase in the chain length of the fatty-acid anion does not influence much in the interaction energy value since the interaction mainly depends on the carboxyl functional group (COO^-). In the case of $[MIM]^+–[C_mH_nCOO]^-$ interactions, the calculated interaction energy value show that among the studied systems the $[MIM]^+–[C_1H_3COO]^-$ has the maximum interaction energy value of -131.55 kcal/mol. Similarly, the $[MIM]^+–[C_1H_3COO]^-$ has the maximum interaction energy value of -139.93 kcal/mol in the water phase (dielectric constant=78.35) (Figure 10). The continuum solvation models are used to study the solvent effects on molecular structure and energetics of ILs. In this study, the calculated solvation energy (ΔG_{sol}) of $[MIM]^+–[C_mH_nCOO]^-$ (m=1–6; n=3–13) are listed in Table 2. For ILs–Water interactions, the calculated total interaction energy values are ranges from -132 kcal/mol to -140 kcal/mol. The calculated interaction energy value shows that the ILs with two water molecules have the strong interaction than the other (i.e. ILs–$1H_2O$ and ILs–$3H_2O$) (Figure 11). The thermodynamic properties such as changes in enthalpy (ΔH) and changes in Gibbs' free energies (ΔG) related to the ILs–Water molecules interaction are calculated and listed in Table 2. From Table 2, it is found that the changes in enthalpy corresponds to ILs–Water interaction is negative (i.e. $\Delta H<0$) which indicates the above interaction is an exothermic in nature.

Table 2
The solvation energy (ΔG_{solv}) and thermodynamic properties such as change in enthalpy and change in Gibbs' free energies corresponding the interactions of $[MIM]^+–[C_mH_nCOO]^-$ (m=1–6; n=3–13) ionic liquids with water clusters $(H_2O)_{1-3}$.

ILs	ΔG_{solv}	ILs–1(H_2O)		ILs–2(H_2O)		ILs–3(H_2O)	
		ΔH	ΔG	ΔH	ΔG	ΔH	ΔG
$[MIM]^+–[C_1H_3COO]^-$	-8.83	-2.64	5.64	-9.90	2.54	-5.38	6.97
$[MIM]^+–[C_2H_5COO]^-$	-8.79	-2.90	6.72	-9.83	3.60	-5.81	6.81
$[MIM]^+–[C_3H_7COO]^-$	-8.53	-3.37	5.26	-10.27	2.81	-5.86	6.67
$[MIM]^+–[C_4H_9COO]^-$	-8.41	-2.71	7.10	-10.07	4.09	-4.93	8.09
$[MIM]^+–[C_5H_{11}COO]^-$	-8.28	-3.54	7.45	-10.44	3.64	-5.48	6.54
$[MIM]^+–[C_6H1_3COO]^-$	-8.28	-2.86	6.29	-10.70	2.81	-5.14	6.88

3.7 AIM analysis

To investigate about the nature of H-bond in the selected ILs, we employ the electron density based topological parameter within the framework of Bader's quantum theory of atoms in molecule (QTAIM)

using MORPHY 98 program [56, 57]. The QTAIM method examines the topology of electron density ρ(r) (in a.u.), Laplacian of electron density $\nabla^2\rho(r)$ (in a.u.) at bond critical point (BCP) and hessian (H_{BCP} = G_{BCP} + V_{BCP}) values and based on the above values the strength of the H-bond can be identified. In general, if the both $\nabla^2\rho(r)$ and H_{BCP} values are positive then the H-bond is weak interaction and if $\nabla^2\rho(r)$ is positive and H_{BCP} is negative then the H-bond is strong. Also, the H_{BCP}>0 indicates the electrostatic interaction and the H_{BCP}<0 indicates the covalent interaction. In this study, the calculated electron density ρ(r), Laplacian of electron density $\nabla^2\rho(r)$ and H_{BCP} values are listed in Table 1. From Table 1, we can found that the H-bond interaction between $[MIM]^+$–$[C_mH_nCOO]^-$ (m=1–6; n=3–13) ILs consist of one strong and one weak H-bond. In our studied $[MIM]^+$ and $[C_mH_nCOO]^-$ (m=1–6;n-3–13) ILs, there are two types of H-bonds are found (*i.e.* N–H···O and C–H···O). Among the two H-bond interactions, the N–H···O interactions corresponds to strong one and the C–H···O interactions corresponds to weaker one. The calculated ρ(r) values ranges from 0.013 to 0.053 a.u. and the $\nabla^2\rho(r)$ value ranges of 0.050–0.105 a.u is observed. Also, the H_{BCP} value is negative for N–H···O interactions and it is positive for C–H···O interactions. The above values suggests that there is one strong H-bond (N–H···O) and one weak H-bond (C–H···O) found between $[MIM]^+$–$[C_mH_nCOO]^-$ (m=1–6; n=3–13) ILs. The result from AIM analysis is in correlation with the H-bond distance between $[MIM]^+$–$[C_mH_nCOO]^-$ (m=1–6; n=3–13) ILs. That is, strong H-bond corresponds to N–H···O interactions (1.70 Å) and the weak H-bond corresponds to C–H···O interactions (2.31 Å).

3.8 NBO analysis

The H-bond formation is associate with certain amount of charge is transferred from the proton donor to the proton acceptor molecule [48]. The NBO analysis is used to understand the charge transfer corresponds to the H-bond formation. In a system with X–H···Y H-bond interaction, the charge transfer takes place between the lone pair of donor (Y) to the anti-bonding orbital σ* (X–H) of acceptor. The stabilization energy $E^{(2)}$ corresponds to Y(LP) ◊ σ* (X–H) H-bond can calculated by, $E^{(2)} = \rho(r_i)\ F(i, j)^2 / E_i – E_j$, where F(i, j) is the off-diagonal or coupling NBO fock matrix element, E_i and E_j are the diagonal elements. In this study, the calculated occupation number of donor and acceptor of ions and the stabilization energy values are listed in Table 3. Here, the $[MIM]^+$–$[C_mH_nCOO]^-$ (m=1–6; n=3–13) interactions lead to change the negative charge on the fatty-acid anion from –1 to –0.59 e/a.u. which means that the charge transfer from anion to cation is 0.41 e/a.u.. The calculated occupancy values show that the occupancies of proton acceptor N (O13) and N (O14) in carboxyl (COO^-) group of fatty-acid anion is decreased by 0.008 a.u. (N–H···O) and 0.002 a.u. (C–H···O) and occupancies of proton donor is increased by 0.068 a.u. (N–H···O) and 0.010 a.u. (C–H···O) during the $[MIM]^+$–$[C_mH_nCOO]^-$ (m=1–6; n=3–13) interactions. The stabilization energy $E^{(2)}$ corresponds to N–H···O interactions is calculated as 36.98–38.51 kcal/mol and it is 1 kcal/mol for the C–H···O interactions. The NBO analysis also results the presence of one strong and one weak H-bond in the $[MIM]^+$–$[C_mH_nCOO]^-$ (m=1–6; n=3–13) ILs.

Table 3
The electron occupancy in H-bond donor N(Y) and acceptor σ*(X–H) units, the stabilization energy corresponds to the H-bond formed between $[MIM]^+$ and $[C_mH_nCOO]^-$ (m=1–6; n=3–13) ionic liquids and the changes in the fatty-acid anionic charge (Δq) during ILs formation.

ILs	Bond type	Donor N(Y)		Acceptor N(σ*(X–H))		$E^{(2)}$	Δq on
		complex	**monomer**	**complex**	**monomer**		Anion
$[MIM]^+–[C_1H_3COO]^-$	N–H···O	1.9701	1.9783	0.0792	0.0108	38.51	-0.5888
	C–H···O	1.9764	1.9786	0.0200	0.0094	1.02	
$[MIM]^+–[C_2H_5COO]^-$	N–H···O	1.9698	1.9789	0.0795	0.0108	38.48	-0.5889
	C–H···O	1.9764	1.9790	0.0201	0.0094	1.06	
$[MIM]^+–[C_3H_7COO]^-$	N–H···O	1.9699	1.9788	0.0786	0.0108	37.96	-0.5882
	C–H···O	1.9762	1.9789	0.0201	0.0094	1.07	
$[MIM]^+–[C_4H_9COO]^-$	N–H···O	1.9695	1.9788	0.0776	0.0108	37.43	-0.5868
	C–H···O	1.9765	1.9789	0.0201	0.0094	1.07	
$[MIM]^+–[C_5H_{11}COO]^-$	N–H···O	1.9695	1.9789	0.0769	0.0108	36.98	-0.5863
	C–H···O	1.9765	1.9788	0.0202	0.0094	1.10	
$[MIM]^+–[C_6H_{13}COO]^-$	N–H···O	1.9695	1.9788	0.0778	0.0108	37.60	-0.5869
	C–H···O	1.9766	1.9789	0.0201	0.0094	1.03	

4. Conclusion

Here in, we employed the DFT calculations for the studies on water aggregation behaviour of methyl-imidazolium cation $[MIM]^+$ with fatty-acid anions $[C_mH_nCOO]^-$ (m=1–6; n=3–13) of ILs. The selected ILs are optimized in both gas phase and water phase. The optimized structures show that the $[MIM]^+–[C_mH_nCOO]^-$ (m=1–6; n=3–13) ILs has one strong (N–H···O) and one weak (C–H···O) H-bond interactions. During the ion-pair formation, the proton transfer process is observed from 'N' atom of $[MIM]^+$ cation to the 'O' atom of fatty-acid anions $[C_mH_nCOO]^-$ (m=1–6; n=3–13). From the vibrational frequency analysis, it is evident that the red-shifted H-bond is found between $[MIM]^+–[C_mH_nCOO]^-$ (m=1–6; n=3–13) ionic liquids. From the interaction energy calculations, it is found that the water molecules (i.e. $(H_2O)_{1-3}$) preferentially interact with fatty-acid based anions rather than methyl-imidazolium cation. Further the ILs–water molecule interactions show that the addition of water molecule reduces the interaction between methyl-imidazolium cation and fatty-acid based anions of ILs. The AIM and NBO analysis also confirms the presence of one strong (N–H···O) and one weak (C–H···O) H-bond interactions between

methyl-imidazolium cation and fatty-acid based anions of ILs. The stabilization energy $E^{(2)}$ corresponds to the proton transfer process (*i.e.* N–H···O interaction) is calculated as 36.98–38.51 kcal/mol.

Declarations

Authors' contributions

The authors, Suresh Sampathkumar and Subramaniam Vijayakumar have contributed to the development of this manuscript and the associated research work and deserve authorship.

Consent to participate

The authors listed are aware and have approved the submission of the article.

Consent for publication

Authors agree on the publication of the article on acceptance of the submission.

Conflicts of interests

The authors have no conflicts of interest to declare that are relevant to the content of this article.

Funding

No funding was received for conducting this study.

Ethics approval

Authors declare that the manuscript satisfy the ethical standards required for publication.

Availability of data and material

The manuscript has no associated data to be deposited.

References

1. Gabriel S, Weiner J (1888) On some derivatives of propylamines. Ber. Dtsch. Chem. Ges 21: 2669-2679.
2. Welton T (1999) Room-temperature ionic liquids. Solvents for synthesis and catalysis. Chem. Rev. 99 (8): 2071-2084.
3. Holbrey JD, Seddon KR (1999) Ionic liquids. Clean products and processes 1 (4): 223-236.
4. Dupont J, de Souza RF, Suarez PAZ (2002) Ionic liquid (molten salt) phase organometallic catalysis. Chem. Rev. 102 (10): 3667-3692.

5. Baudequin C, Baudoux J, Levillain J, Cahard D, Gaumont AC, Plaquevent JC (2003) Ionic liquids and chirality: opportunities and challenges. Tetrahedron: Asymmetry 14 (20): 3081-3093.
6. Bao W, Wang Z, Li Y (2003) Synthesis of chiral ionic liquids from natural amino acids. J. Org. Chem. 68 (2): 591-593.
7. Wasserscheid P, Welton T (2008) Ionic liquids in synthesis. John Wiley & Sons.
8. Weingärtner H (2008) Understanding ionic liquids at the molecular level: facts, problems, and controversies. Angew. Chem. Int. Ed. 47 (4): 654-670.
9. Zhou Y (2005) Recent advances in ionic liquids for synthesis of inorganic nanomaterials. Curr. Nanosci. 1 (1): 35-42.
10. Nockemann P, Binnemans K, Driesen K (2005) Purification of imidazolium ionic liquids for spectroscopic applications. Chem. Phys. Lett. 415 (1-3): 131-136.
11. Pârvulescu VI, Hardacre C (2007) Catalysis in ionic liquids. Chem. Rev. 107 (6): 2615-2665.
12. Dyson PJ, Geldbach TJ (2007) Applications of ionic liquids in synthesis and catalysis. Interface-Electrochemical Society 16 (1): 50-53.
13. Harjani JR, Singer RD, Garcia MT, Scammells PJ (2009) Biodegradable pyridinium ionic liquids: design, synthesis and evaluation. Green Chem. 11 (1): 83-90.
14. Atefi F, Garcia MT, Singer, RD, Scammells PJ (2009) Phosphonium ionic liquids: design, synthesis and evaluation of biodegradability. Green Chem. 11 (10): 1595-1604.
15. Aparicio S, Atilhan M, Karadas F (2010) Thermophysical properties of pure ionic liquids: review of present situation. Ind. Eng. Chem. Res. 49 (20): 9580-9595.
16. Hallett JP, Welton T (2011) Room-temperature ionic liquids: solvents for synthesis and catalysis. 2. Chem. Rev. 111 (5): 3508-3576.
17. Dong K, Zhang S (2012) Hydrogen bonds: a structural insight into ionic liquids. Chem. Eur. J 18 (10): 2748-2761.
18. Yang Q, Xu D, Zhang J, Zhu Y, Zhang Z, Qian C, Ren Q, Xing H (2015) Long-chain fatty acid-based phosphonium ionic liquids with strong hydrogen-bond basicity and good lipophilicity: synthesis, characterization, and application in extraction. ACS Sustainable Chem. Eng. 3 (2): 309-316.
19. Rocha MAA, van den Bruinhorst A, Schröer W, Rathke B, Kroon MC (2016) Physicochemical properties of fatty acid based ionic liquids. J. Chem. Thermodyn. 100: 156-164.
20. Wasserscheid P, Keim W (2000) Ionic liquids—new “solutions” for transition metal catalysis. Angew. Chem. Int. Ed. 39 (21): 3772-3789.
21. Wang P, Zakeeruddin SM, Moser JE, Nazeeruddin MK, Sekiguchi T, Grätzel M (2003) A stable quasi-solid-state dye-sensitized solar cell with an amphiphilic ruthenium sensitizer and polymer gel electrolyte. Nat. Mater. 2 (6): 402-407.
22. Song CE (2004) Enantioselective chemo-and bio-catalysis in ionic liquids. Chem. Commun. 9: 1033-1043.

23. Buzzeo MC, Evans RG, Compton RG (2004) Non-haloaluminate room-temperature ionic liquids in electrochemistry-a review. ChemPhysChem 5 (8): 1106-1120.
24. Ni X, Xing H, Yang Q, Wang J, Su B, Bao Z, Yang Y, Ren Q (2012) Selective liquid–liquid extraction of natural phenolic compounds using amino acid ionic liquids: a case of α-tocopherol and methyl linoleate separation. Ind. Eng. Chem. Res. 51 (18): 6480-6488.
25. Chen X, Li F, Asumana C, Yu G (2013) Extraction of soluble dyes from aqueous solutions with quaternary ammonium-based ionic liquids. Sep. Purif. Technol. 106: 105-109.
26. Vander Hoogerstraete T, Binnemans K (2014) Highly efficient separation of rare earths from nickel and cobalt by solvent extraction with the ionic liquid trihexyl (tetradecyl) phosphonium nitrate: a process relevant to the recycling of rare earths from permanent magnets and nickel metal hydride batteries. Green Chem. 16 (3): 1594-1606.
27. Fukumoto K, Yoshizawa M, Ohno H (2005) Room temperature ionic liquids from 20 natural amino acids. J. Am. Chem. Soc. 127 (8): 2398-2399.
28. Manojkumar K, Sivaramakrishna A, Vijayakrishna K (2016) A short review on stable metal nanoparticles using ionic liquids, supported ionic liquids, and poly (ionic liquids). J. Nanopart. Res. 18 (4): 103.
29. Qian W, Texter J, Yan F (2017) Frontiers in poly (ionic liquid) s: syntheses and applications. Chem. Soc. Rev. 46 (4): 1124-1159.
30. Tao GH, He L, Liu WS, Xu L, Xiong W, Wang T, Kou Y (2006) Preparation, characterization and application of amino acid-based green ionic liquids. Green Chem. 8 (7): 639-646.
31. Li T, Yang Q, Ding H, Li J, Peng C, Liu H (2015) Amino acid based ionic liquids as additives for the separation of an acetonitrile and water azeotropic mixture: COSMO-RS prediction and experimental verification. Ind. Eng. Chem. Res. 54 (48): 12143-12149.
32. Shyama M, Lakshmipathi S (2020) Water confined (H2O) n= 1–10 amino acid-based ionic liquids–A DFT study on the bonding, energetics and IR spectra. J. Mol. Liq. 304: 112720.
33. Giernoth R (2010) Task-Specific Ionic Liquids. Angew. Chem. Int. Ed. 49 (16): 2834-2839.
34. Yuvaraj SVJ, Zhdanov RK, Belosludov RV, Belosludov VR, Subbotin OS, Kanie K, Funaki K, Muramatsu A, Nakamura T, Kawazoe Y (2015) Solvation mechanism of task-specific ionic liquids in water: a combined investigation using classical molecular dynamics and density functional theory. J. Phys. Chem. B 119 (40): 12894-12904.
35. Bera A, Belhaj H (2016) Ionic liquids as alternatives of surfactants in enhanced oil recovery—A state-of-the-art review. J. Mol. Liq. 224: 177-188.
36. Šarac B, Medoš Ž, Cognigni A, Bica K, Chen LJ, Bešter-Rogač M (2017) Thermodynamic study for micellization of imidazolium based surface active ionic liquids in water: Effect of alkyl chain length and anions. Colloids Surf., A 532: 609-617.
37. Čobanov I, Šarac B, Medoš Ž, Vraneš M, Gadžurić S, Zec N, Bešter-Rogač M (2018) Effect of cationic structure of surface active ionic liquids on their micellization: A thermodynamic study. J. Mol. Liq. 271: 437-442.

38. Mezzetta A, Łuczak J, Woch J, Chiappe C, Nowicki J, Guazzelli L (2019) Surface active fatty acid ILs: Influence of the hydrophobic tail and/or the imidazolium hydroxyl functionalization on aggregates formation. J. Mol. Liq. 289: 111155.
39. Qin M, Zhong F, Sun Y, Tan X, Hu K, Zhang H, Kong M, Wang G, Zhuang L (2020) Effect of cation substituent of dodecanesulfate-based anionic surface active ionic liquids on micellization: Experimental and theoretical studies. J. Mol. Liq. 303: 112695.
40. Brown P, Butts CP, Eastoe J, Fermin D, Grillo I, Lee HC, Parker D, Plana D, Richardson RM (2012) Anionic Surfactant Ionic Liquids with 1-Butyl-3-methyl-imidazolium Cations: Characterization and Application. Langmuir 28 (5): 2502-2509.
41. Trush MM, Semenyuta IV, Vdovenko SI, Rogalsky SP, Lobko EO, Metelytsia LO (2017) Synthesis, spectroscopic and molecular docking studies of imidazolium and pyridinium based ionic liquids with HSA as potential antimicrobial agents. J. Mol. Struct. 1137: 692-699.
42. Pillai P, Kumar A, Mandal A (2018) Mechanistic studies of enhanced oil recovery by imidazolium-based ionic liquids as novel surfactants. J. Ind. Eng. Chem. 63: 262-274.
43. Barman BK, Rajbanshi B, Yasmin A, Roy MN (2018) Exploring inclusion complexes of ionic liquids with α- and β- cyclodextrin by NMR, IR, mass, density, viscosity, surface tension and conductance study. J. Mol. Struct. 1159: 205-215.
44. Elaiwi A, Hitchcock PB, Seddon KR, Srinivasan N, Tan YM, Welton T, Zora JA (1995) Hydrogen bonding in imidazolium salts and its implications for ambient-temperature halogenoaluminate(III) ionic liquids. J. Chem. Soc., Dalton Trans. 21: 3467-3472.
45. Fumino K, Wulf A, Ludwig R (2009) Hydrogen Bonding in Protic Ionic Liquids: Reminiscent of Water. Angew. Chem. Int. Ed. 48 (17): 3184-3186.
46. Fumino K, Wulf A, Ludwig R (2009) The potential role of hydrogen bonding in aprotic and protic ionic liquids. Phys. Chem. Chem. Phys. 11 (39): 8790-8794.
47. Fumino K, Peppel T, Geppert-Rybczyńska M, Zaitsau DH, Lehmann JK, Verevkin SP, Köckerling M, Ludwig R (2011) The influence of hydrogen bonding on the physical properties of ionic liquids. Phys. Chem. Chem. Phys. 13 (31): 14064-14075.
48. Hunt PA, Ashworth CR, Matthews RP (2015) Hydrogen bonding in ionic liquids. Chem. Soc. Rev. 44 (5): 1257-1288.
49. Nowicki J, Woch J, Łuczak J, Zarębska M, Nowakowska-Bogdan E, Mościpan M (2018) Micellar Route of the Synthesis of Alkyl Xylosides: An Unexpected Effect of Amphiphilic Imidazolium Ionic Liquids. ChemistrySelect 3 (19): 5254-5262.
50. Wang D, Richter C, Rühling A, Drücker P, Siegmund D, Metzler-Nolte N, Glorius F, Galla HJ (2015) A Remarkably Simple Class of Imidazolium-Based Lipids and Their Biological Properties. Chem. Eur. J 21 (43): 15123-15126.
51. Qin M, Zhong F, Sun Y, Tan X, Hu K, Zhang H, Kong M, Wang G, Zhuang L (2020) Experimental and DFT studies on surface properties of sulfonate-based surface active ionic liquids. J. Mol. Struct. 1215: 128258.

52. Zhao Y, Truhlar DG (2008) The M06 suite of density functionals for main group thermochemistry, thermochemical kinetics, noncovalent interactions, excited states, and transition elements: two new functionals and systematic testing of four M06-class functionals and 12 other functionals. Theor. Chem. Acc. 120 (1-3): 215-241.
53. Frisch MJ, Pople JA, Binkley JS (1984) Self-consistent molecular orbital methods 25. Supplementary functions for Gaussian basis sets. J. Chem. Phys. 80 (7): 3265-3269.
54. Miertuš S, Scrocco E, Tomasi J (1981) Electrostatic interaction of a solute with a continuum. A direct utilizaion of AB initio molecular potentials for the prevision of solvent effects. Chem. Phys. 55 (1): 117-129.
55. Tomasi J, Mennucci B, Cammi R (2005) Quantum mechanical continuum solvation models. Chem. Rev. 105 (8): 2999-3094.
56. Bader RFW (1991) A quantum theory of molecular structure and its applications. Chem. Rev. 91 (5): 893-928.
57. Popelier PLA (1994) An analytical expression for interatomic surfaces in the theory of atoms in molecules. Theor. Chim. Acta 87 (6): 465-476.
58. Weinhold F (2012) Natural bond orbital analysis: a critical overview of relationships to alternative bonding perspectives. J. Comput. Chem. 33 (30): 2363-2379.
59. Frisch MJ, Trucks GW, Schlegel HB, Scuseria GE, Robb MA, Cheeseman JR, Scalmani G, Barone V, Mennucci B, Petersson GA, Nakatsuji H, Li X, Caricato M, Hratchian HP, Izmaylov AF, Bloino J, Zheng G, Sonnenberg JL, Hada M, Ehara M, Toyota K, Fukuda R, Hasegawa J, Ishida M, Nakajima T, Honda Y, Kitao O, Nakai H, Vreven T, Montgomery JA, Jr., Peralta JE, Ogliaro F, Bearpark M, Heyd JJ, Brothers E, Kudin KN, Staroverov VN, Kobayashi R, Normand J, Raghavachari K, Rendell A, Burant JC, Iyengar SS, Tomasi J, Cossi M, Rega N, Millam JM, Klene M, Knox JE, Cross JB, Bakken V, Adamo C, Jaramillo J, Gomperts R, Stratmann RE, Yazyev O, Austin AJ, Cammi R, Pomelli C, Ochterski JW, Martin RL, Morokuma K, Zakrzewski VG, Voth GA, Salvador P, Dannenberg JJ, Dapprich S, Daniels AD, Farkas O, Foresman JB, Ortiz JV, Cioslowski J, Fox, DJ (2009) Gaussian 09, Revision A.02, Wallingford CT.
60. Hunt PA, Kirchner B, Welton T (2006) Characterising the electronic structure of ionic liquids: an examination of the 1-butyl-3-methylimidazolium chloride ion pair. Chem. Eur. J 12 (26): 6762-6775.
61. Xu W, Wang T, Cheng N, Hu Q, Bi Y, Gong Y, Yu L (2015) Experimental and DFT studies on the aggregation behavior of imidazolium-based surface-active ionic liquids with aromatic counterions in aqueous solution. Langmuir 31 (4): 1272-1282.
62. Roohi H, Khyrkhah S (2015) Quantum chemical studies on nanostructures of the hydrated methylimidazolium–based ionic liquids. J. Mol. Model. 21 (1): 1.
63. Ali MK, Moshikur RM, Wakabayashi R, Tahara Y, Moniruzzaman M, Kamiya N, Goto M (2019) Synthesis and characterization of choline–fatty-acid-based ionic liquids: A new biocompatible surfactant. J. Colloid Interface Sci. 551: 72-80.

64. Yamada T, Tominari Y, Tanaka S, Mizuno M (2017) Infrared spectroscopy of ionic liquids consisting of imidazolium cations with different alkyl chain lengths and various halogen or molecular anions with and without a small amount of water. J. Phys. Chem. B 121 (14): 3121-3129.
65. Bellocq AM, Perchard C, Novak A, Josien ML (1965) Spectres de vibration de l'imidazole, de l'imidazole (D)-1, de l'imidazole (D3)-2, 4, 5 et de l'imidazole (D4)-Partie I: Région entre 4 000 et 1 700 cm−1. Journal de Chimie Physique 62: 1334-1343.
66. Voss JM, Marsh BM, Zhou J, Garand E (2016) Interaction between ionic liquid cation and water: Infrared predissociation study of $[bmim]^+.(H_2O)n$ clusters. Phys. Chem. Chem. Phys. 18 (28): 18905-18913.

Figures

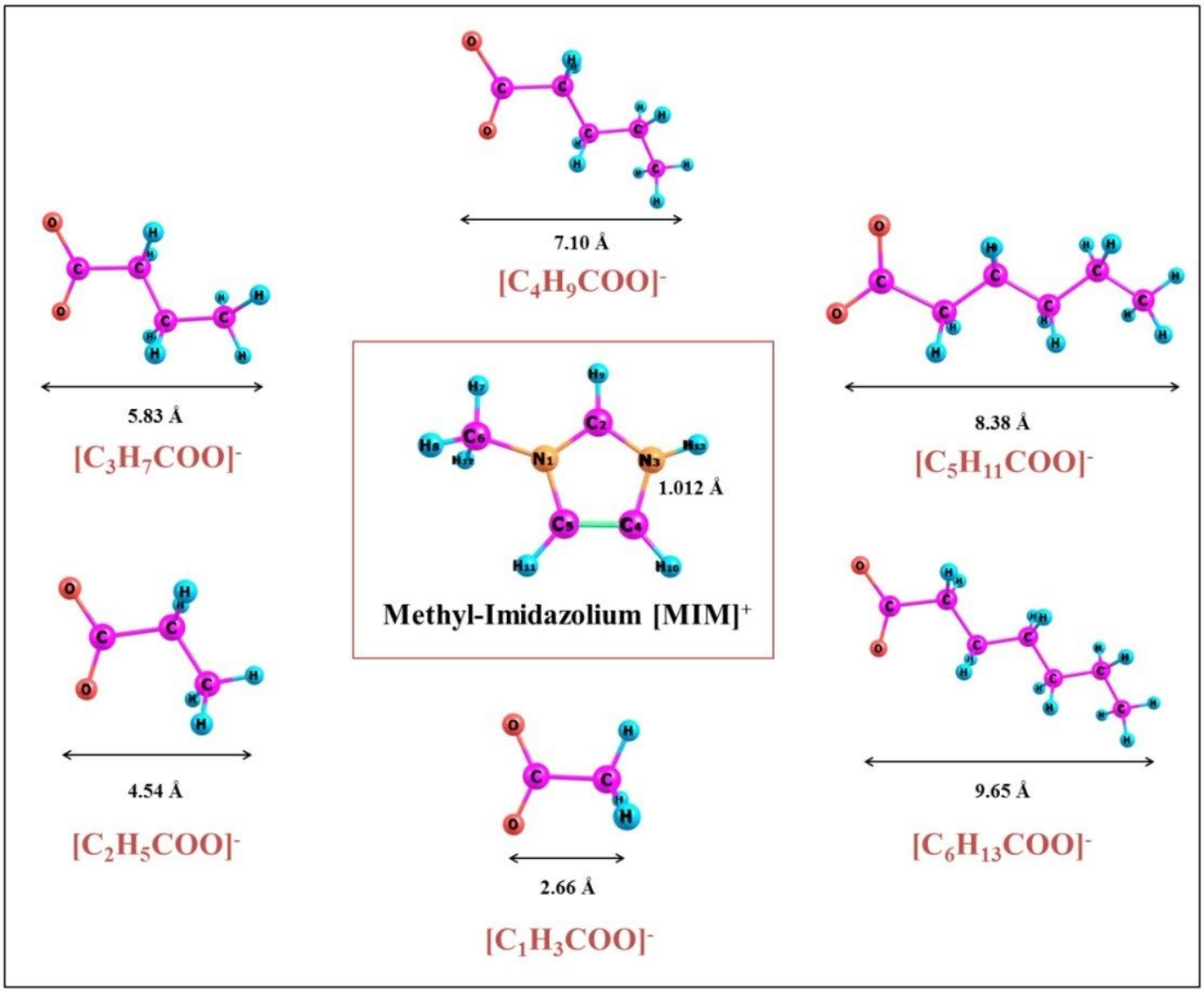

Figure 1

The optimized structures of methyl-imidazolium cation [MIM]+ and fatty-acid anions [CmHnCOO]- (m=1-6; n=3-13) with their chain length calculated at M06-2X/6-311++G** level of theory.

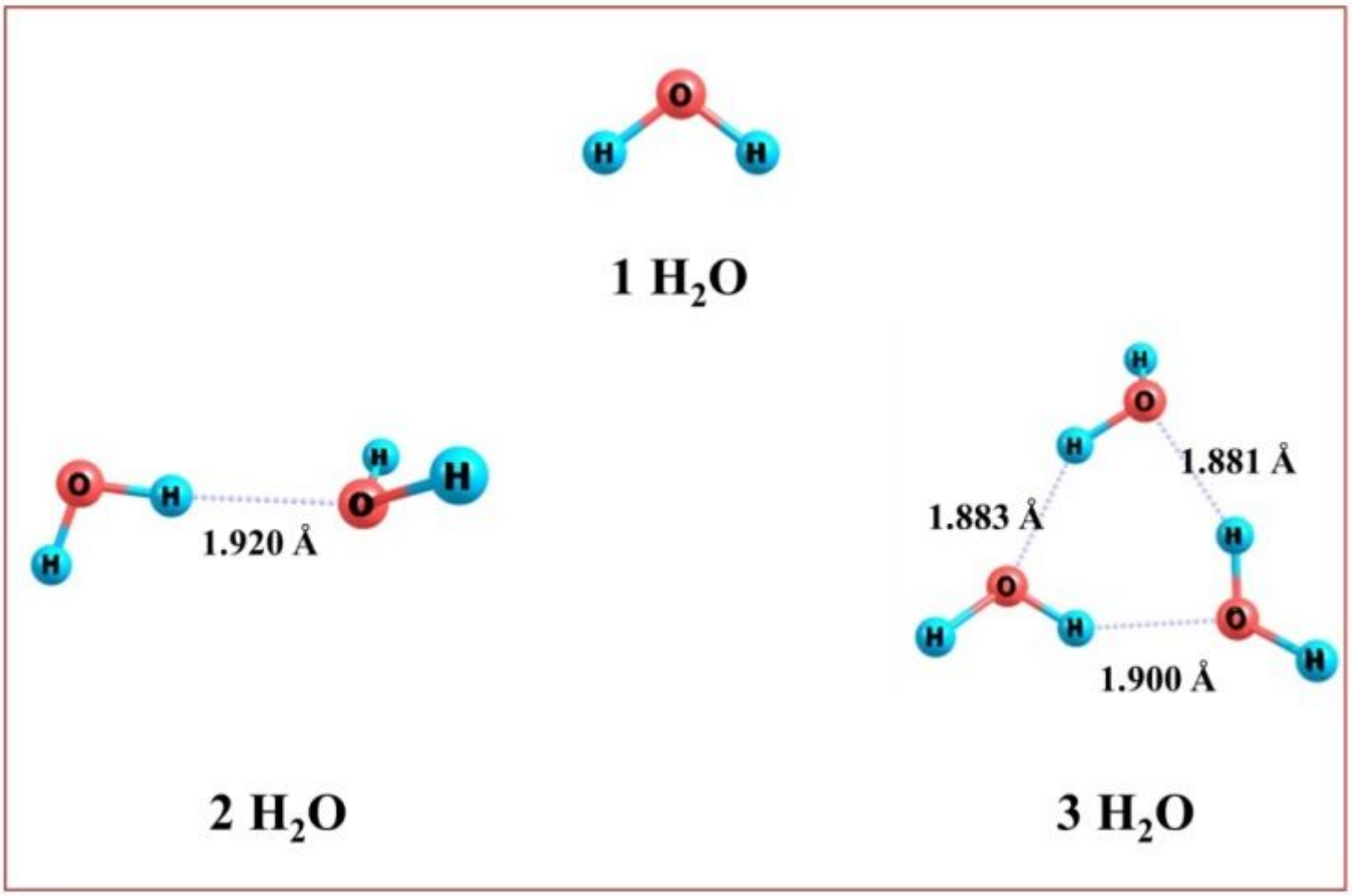

Figure 2

The optimized water cluster (H2O)x (x=1-3) at M06-2X/6-311++G** level of theory.

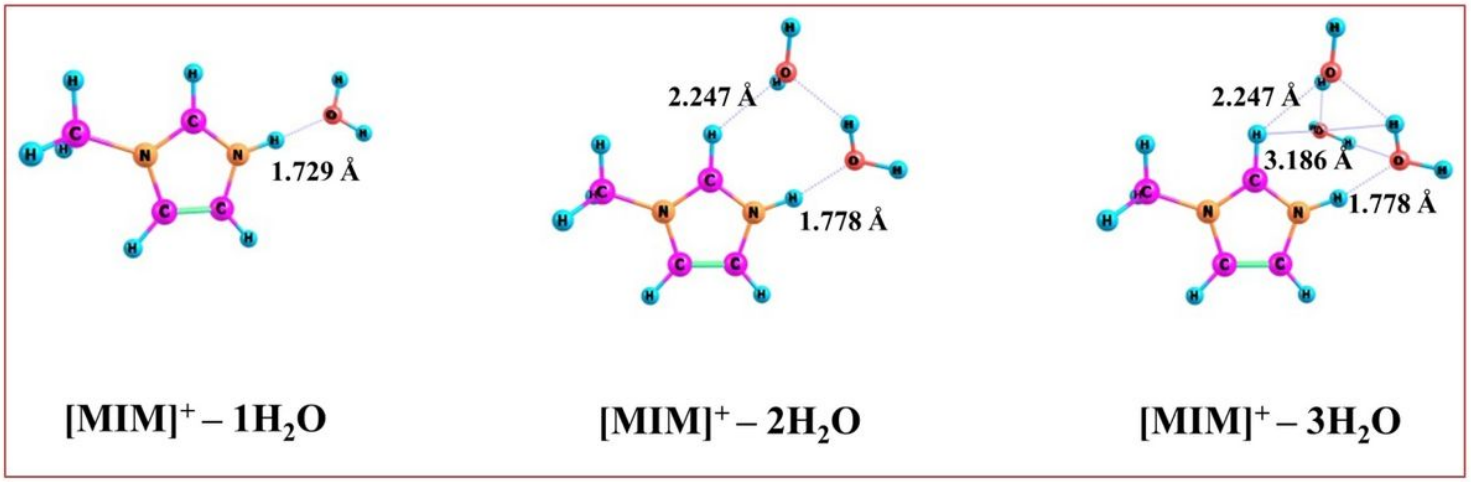

Figure 3

The optimized structures of methyl-imidazolium cation [MIM]+ with water cluster (H2O)x (where, x=1-3) at M06-2X/6-311++G** level of theory.

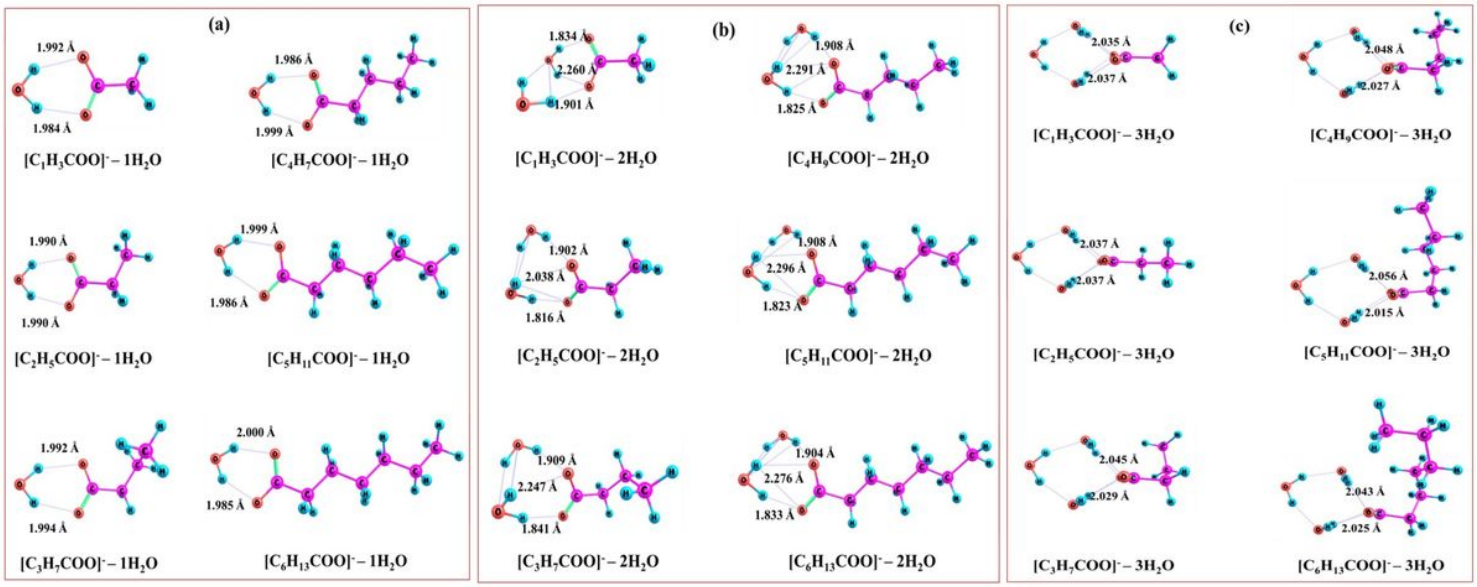

Figure 4

The optimized structures of fatty-acid anions [CmHnCOO]- (m=1=6; n=3-13) with water cluster (a) (H2O)1, (b) (H2O)2 and (c) (H2O)3 at M06-2X/6-311++G** level of theory.

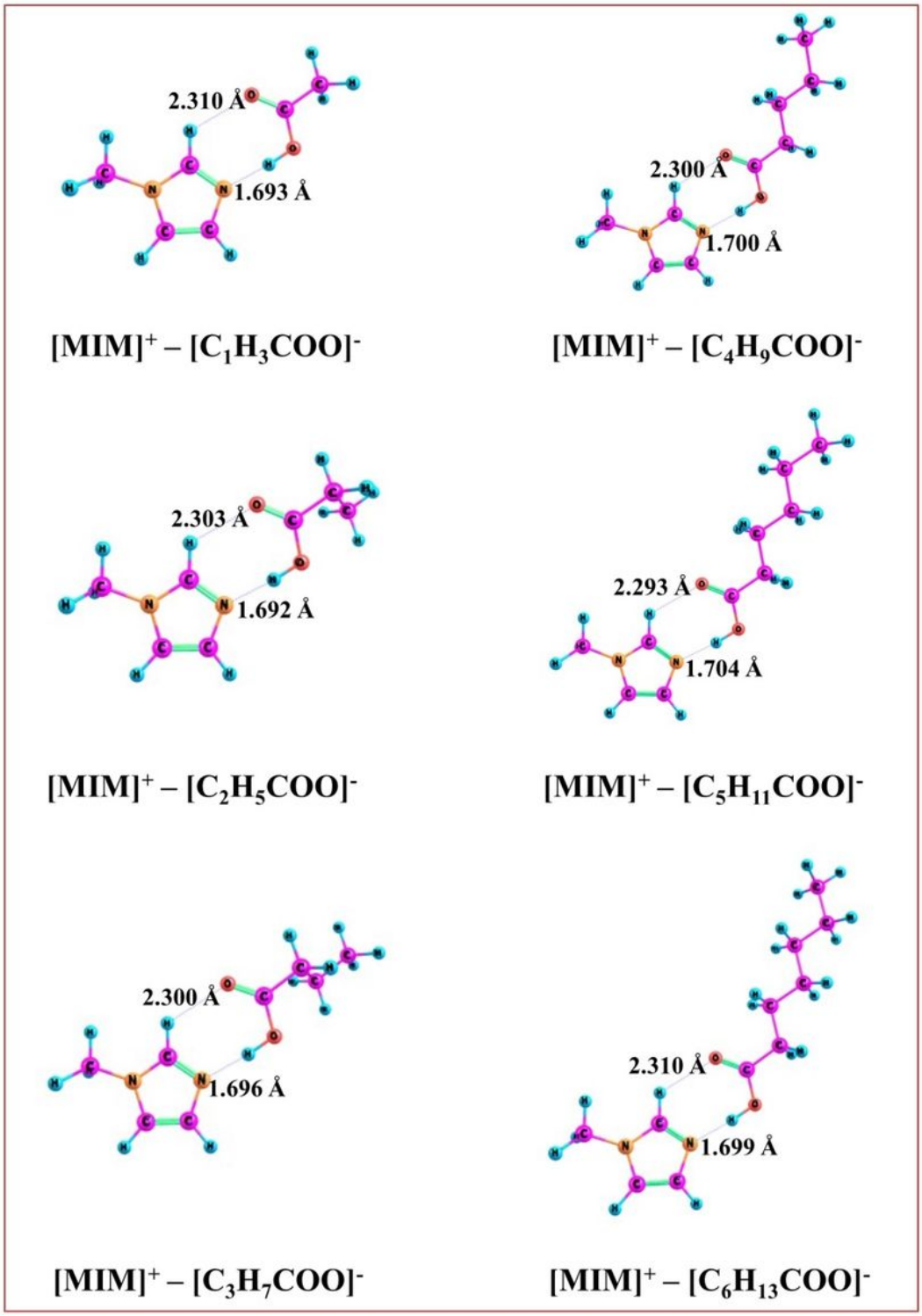

Figure 5

The optimized structures of ILs [MIM]+–[CmHnCOO]- (where, m=1-6; n=3-13) at M06-2X/6-311++G** level of theory (site-1).

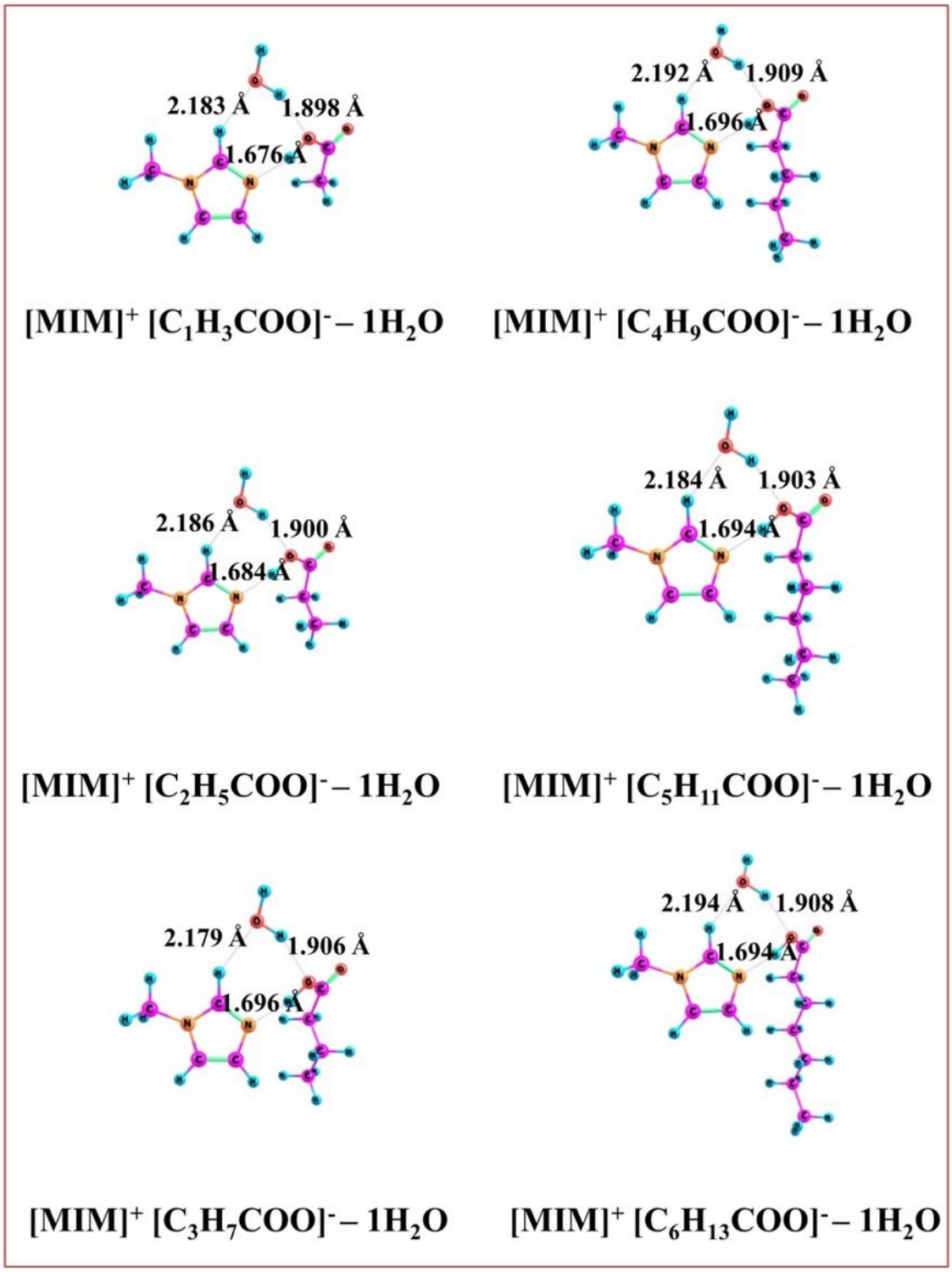

Figure 6

The optimized structures of ILs [MIM]+–[CmHnCOO]- (where, m=1-6; n=3-13) with one water molecule (H2O) at M06-2X/6-311++G** level of theory.

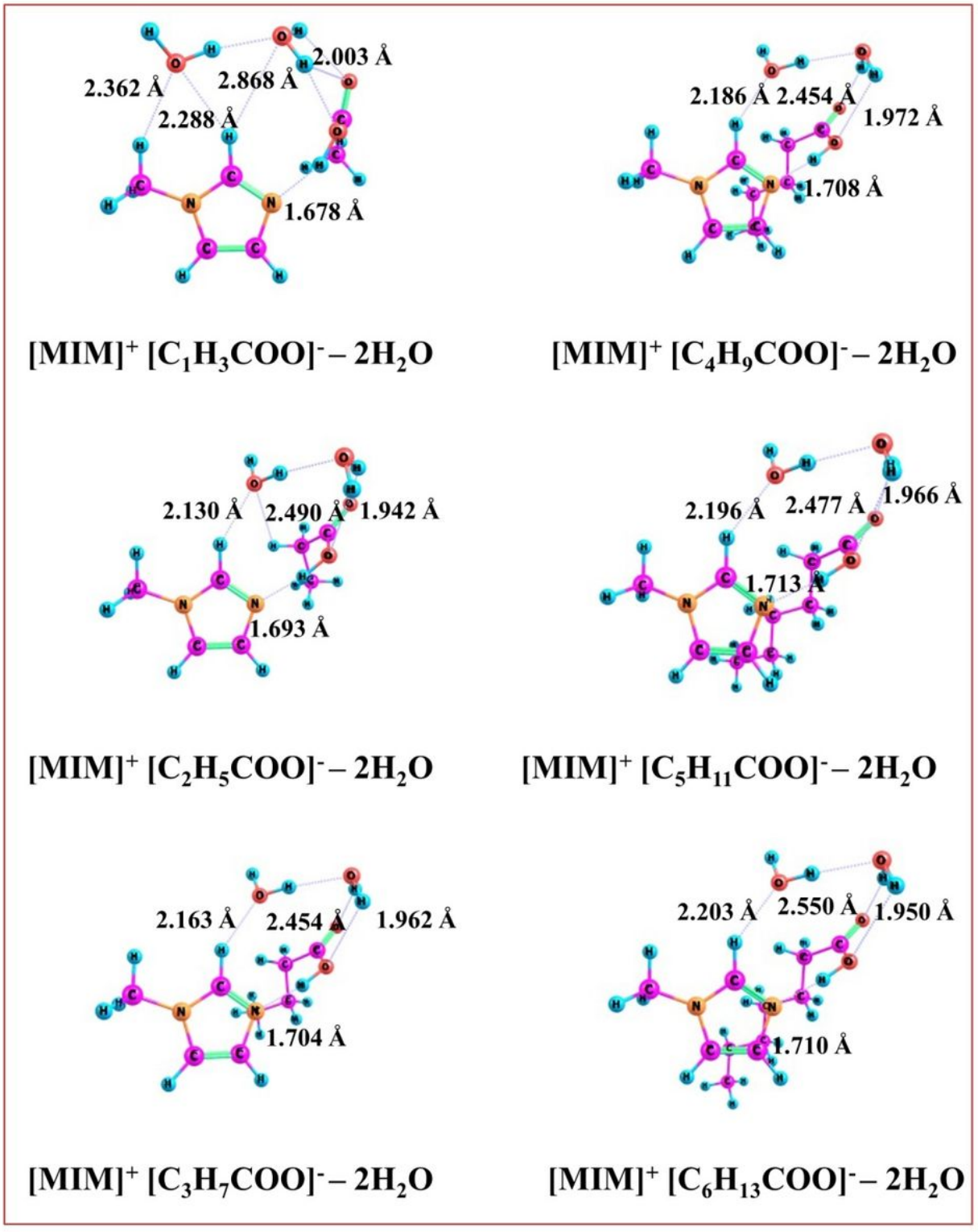

Figure 7

The optimized structures of ILs [MIM]+–[CmHnCOO]- (where, m=1-6; n=3-13) with two water molecules (H2O)2 at M06-2X/6-311++G** level of theory.

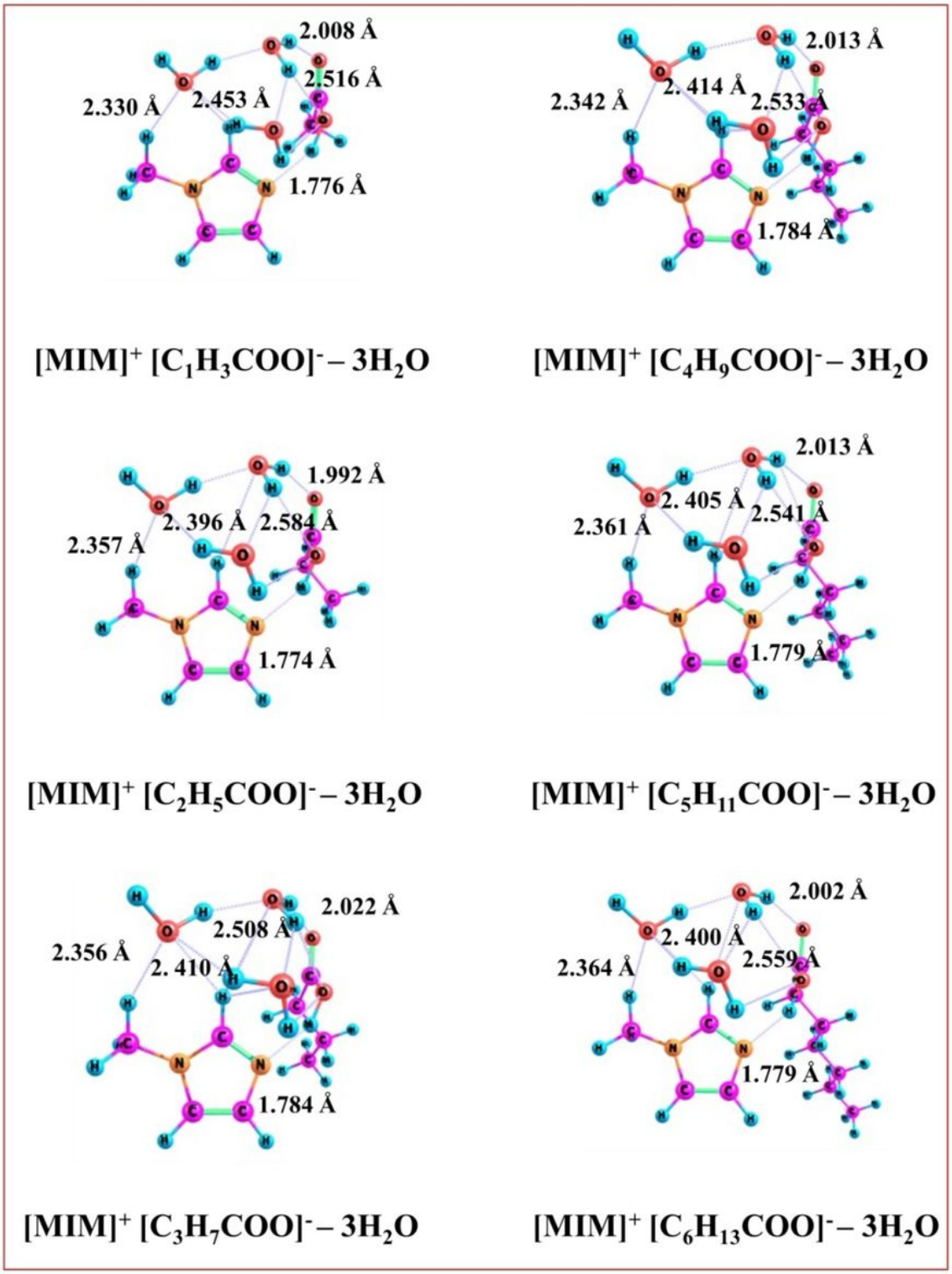

Figure 8

The optimized structures of Ion-pairs [MIM]+–[CmHnCOO]- (m=1-6; n=3-13) with three water molecules (H2O)3 at M06-2X/6-311++G** level of theory.

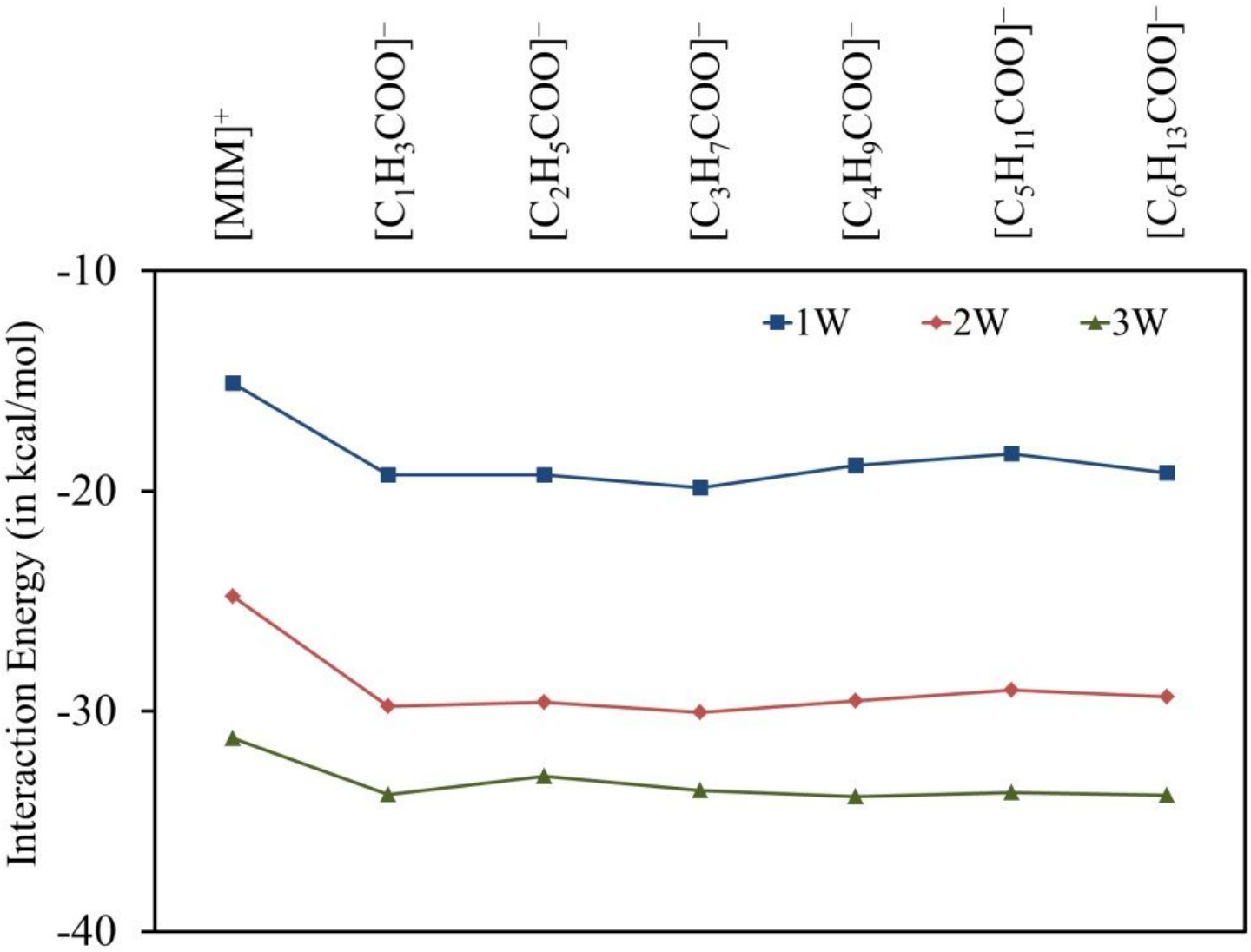

Figure 9

The interaction energy of [MIM]+ cation and [CmHnCOO]- (m=1=6; n=3-13) anions with water clusters (H2O)1-3. (1W denotes (H2O)1, 2W denotes (H2O)2 and 3W denotes (H2O)3)

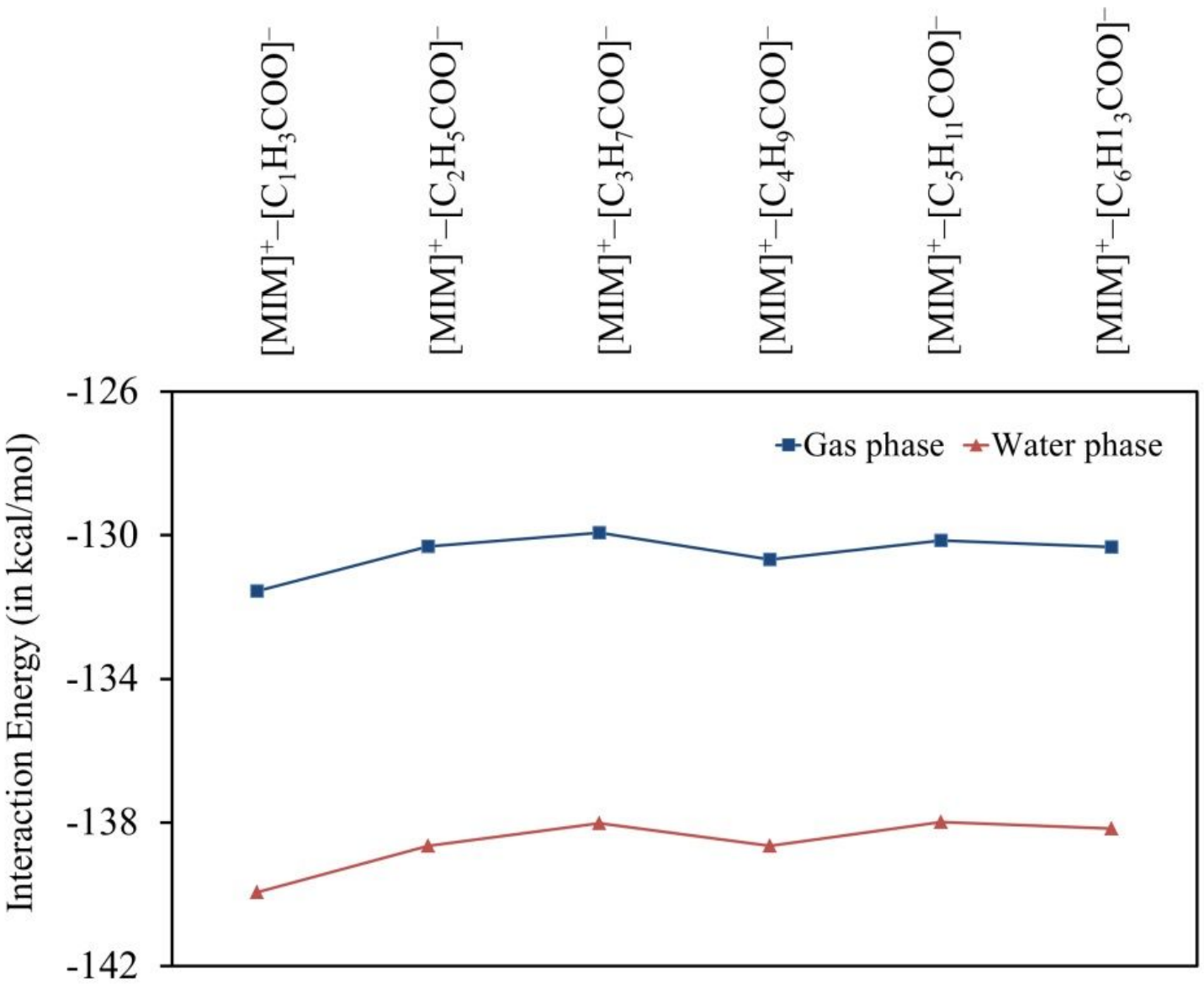

Figure 10

The interaction between [MIM]+–[CmHnCOO]- (m=1-6; n=3-13) in gas phase and water phase.

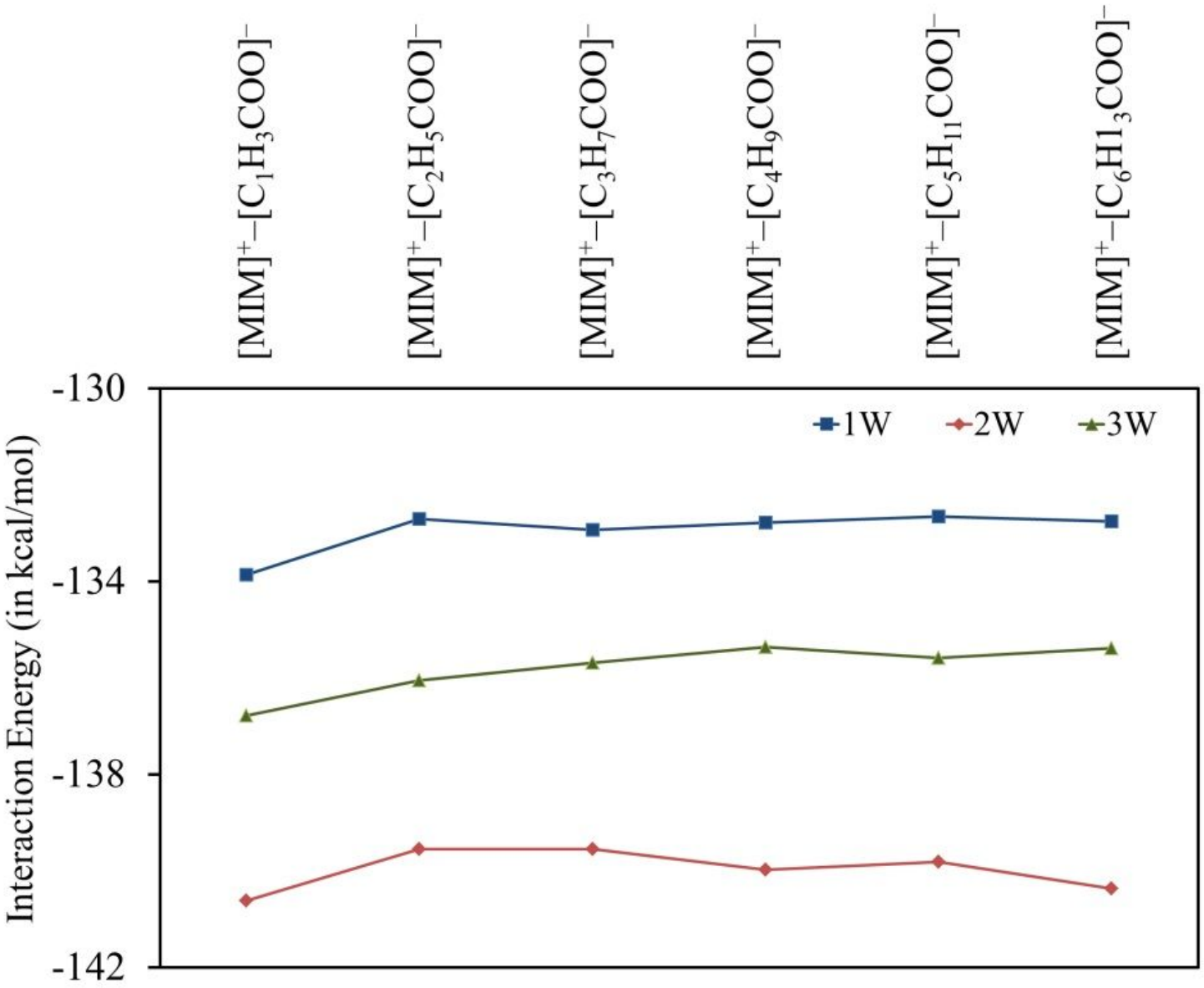

Figure 11

The interaction energy between [MIM]+–[CmHnCOO]- (m=1-6; n=3-13) with water clusters (H2O)1-3. (1W denotes (H2O)1, 2W denotes (H2O)2 and 3W denotes (H2O)3)

Supplementary Files

This is a list of supplementary files associated with this preprint. Click to download.

- GraphicalAbstract.docx
- SupportingInformation.docx